Research Square

Preprints are preliminary reports that have not undergone peer review.
They should not be considered conclusive, used to inform clinical practice,
or referenced by the media as validated information.

CO_2 adsorption and CO_2/CH_4 separation using fibrous amine-containing adsorbents: isothermal, kinetic and thermodynamic behaviours

Noor Ashikin Mohamad
Universiti Teknologi Malaysia - Kampus Kuala Lumpur
Mohamed Mahmoud Nasef (mahmoudeithar@cheme.utm.my)
Universiti Teknologi Malaysia https://orcid.org/0000-0002-0192-5107
Tuan Amran Tuan Abdullah
Universiti Teknologi Malaysia - Main Campus Skudai: Universiti Teknologi Malaysia
Arshad Bin Ahmad
Universiti Teknologi Malaysia - Main Campus Skudai: Universiti Teknologi Malaysia
Teo Ming Ting
Malaysian Nuclear Agency: Agensi Nuklear Malaysia

Research Article

Keywords: Fibrous adsorbent, Aminated poly (glycidyl methacrylate chains, CO2 adsorption isotherms, Kinetic behaviour, Thermodynamic analysis, Natural gas purification

Posted Date: January 24th, 2023

DOI: https://doi.org/10.21203/rs.3.rs-2430401/v1

License: This work is licensed under a Creative Commons Attribution 4.0 International License.
Read Full License

Version of Record: A version of this preprint was published at Environmental Science and Pollution Research on May 1st, 2023. See the published version at https://doi.org/10.1007/s11356-023-26913-6.

Abstract

A series of fibrous aminated adsorbents for CO_2 adsorption were prepared by covalent incorporation of poly (glycidyl methacrylate) (PGMA) by graft copolymerization of GMA onto electron beam (EB) irradiated polyethylene/polypropylene (PE/PP) fibrous sheets and subsequent amination with ethylenediamine (EDA), diethylenetriamine (DETA) or tetraethylenepentamine (TEPA). The physico-chemical properties of the adsorbents were evaluated using Fourier transform infrared spectroscopy (FTIR), scanning electron microscopy (SEM), X-ray diffraction (XRD), thermogravimetric (TGA) and Brunauer-Emmett-Teller (BET) analysis. Of all adsorbents, TEPA-containing fibres showed the highest CO_2 adsorption capacity and thus was further investigated for CO_2 capture from CO_2/CH_4 mixtures of different gas ratios under various pressures and temperatures. The selectivity of CO_2 over CH_4 and equilibrium isotherms, kinetics, and thermodynamics of the adsorption on the fibrous aminated adsorbent were all investigated. The Sips model was found to best fit the isotherm of CO_2 adsorption suggesting the presence of a combination of monolayer and multilayer adsorptions. The adsorption kinetic data was found to best fit Elovich model reflecting chemisorption. The $\Delta G°$, $\Delta S°$, and $\Delta H°$ showed positive values suggesting that the adsorption of CO_2 on the present fibrous adsorbent was non-spontaneous with an increase in randomness implying that the process was endothermic. Overall, it can be suggested that PE/PP-*g*-PGMA/TEPA adsorbent has a strong potential for separation of CO_2 from NG.

Introduction

Natural gas (NG) is the one of cleanest, safest, and most efficient fossil fuel, which emits roughly 26–41% less CO_2 than oil and coal (Adewole et al. 2013). Hence, the demands on NG keep growing with an expected 64% more consumption in the coming few decades. To meet the expanding global demand for NG, offshore NG fields offers an alternative reserves to onshore counterparts and the ocean provides about one-third of global NG (Chen et al. 2017). For offshore NG production, a complete production process is carried out on-site of the floating liquefied NG production storage and off-loading (LNG-FPSO) structures, including pre-treatment, liquefaction, storage, transportation, and off-loading (Chen et al. 2020). The pre-treatment is the most crucial section of the offshore NG development to remove impurities from raw NG before commercializing it. Raw NG comes with high compositions of methane while CO_2 and H_2S are the major impurities (Adewole et al. 2013). Raw NG contains up to 70% of CO_2 depending on the geographical location, and the removal procedure is typically performed at a pressure range of 30–60 bar (Han and Ho 2021). Such high amounts of CO_2 in the NG stream reduce its energy content (calorific values) and create corrosion problems during transportation in pipelines and cylinders. Thus, CO_2 content should be minimized to 2–3% by volume (Lee et al. 2018).

To date, the leading technologies for CO_2 removal from NG are solvent scrubbing, adsorption, membranes separation, and cryogenic distillation. Among all, amine-scrubbing in a gas-liquid contactor is the most mature and commercially used method for CO_2 removal, that offers higher capture efficiency (Mukhtar et al. 2020c). However, this process is high energy demanding, high operational cost, and operates in central

plants making it not suitable for offshore NG treatment (Adewole et al. 2013; Chen et al. 2020). Adsorption technology offers alternative simplified operation, low energy demand, ease of control, and high efficiency in addition to wide range of adsorbent materials (Chen et al. 2020). Broadly, different types of solid adsorbents have been explored for CO_2 capture from NG, including carbon-based materials (Attia et al. 2020), zeolites (Wang et al. 2019), mesoporous silica (Ullah et al. 2015), microporous organic polymer (MOPs) (Xu et al. 2020) and metal-organic framework (MOFs) (Furukawa et al. 2010). All of such adsorbents are packed in fixed bed column for practical applications and this is accompanied by pressure loss, channelling, and inhomogeneous gas flow when fitted for working in the adsorption columns processes such as pressure or temperature swing adsorption (Mallick et al. 2018). Moreover, MOFs bearing extraordinary CO_2 adsorption capacity have high cost, low hydrothermal stability and are not practical for column system at a large scale of LNG-FPSO (Abid et al. 2012; Danaci et al. 2015).

Solid basic polymer adsorbents containing groups such as hydroxy, nitro, amine, imidazole, triazine, and imine provide alternative materials for CO_2 capture (Petrovic et al. 2021). Particularly, the development of new adsorbents with amine-containing fibrous structures provides advantages in terms of rapid gas diffusion and enhanced gas-solid interaction while reducing pressure loss during gas treatment. Graft copolymerization is one of the most appealing methods to impart permanent functional groups to polymer substrates (non-woven fabrics, films, and porous particles) to prepare CO_2 polymer adsorbents with various morphologies (Zhao et al. 2020). Graft copolymerization can be initiated on polymer substrates using high energy radiation including gamma rays, electron beam, low energy radiation such as ultraviolet (UV), and plasma treatment in addition to conventional chemical initiators in the presence of vinyl monomers that can host different amine groups (Shoushtari et al. 2012).

Fibrous amine containing adsorbents is a class of solid polymer adsorbents that have potential to overcome the pressure drop and gas channelling problems when packed in adsorption columns and thus they are worthy further development. Moreover, most of these aminated fibrous adsorbents were tested for CO_2 capture from air and post-combustion effluent despite the presence of other major applications involving NG purification. Fibrous adsorbents were mainly prepared by radiation induced graft copolymerization (RIGC) of vinyl monomers onto polymer non-woven sheets made of polypropylene and polyethylene/polypropylene (PE/PP) (Nasef et al. 2014; Kavaklı et al. 2016; Rojek et al. 2017; Abbasi et al. 2018). Monomers such as glycidyl methacrylate (GMA) (Imanian et al. 2022), N-vinylformamide (Zubair et al. 2020), and acrylamide (Nasef and Güven 2012) were used to endow variety of amine groups after post-grafting treatments and demonstrated an appealing affinity to CO_2 (Nasef and Güven 2012). Applying RIGC for immobilization of functional groups offers advantages in terms of ability to control the level, location, and distribution of graft chains on the substrate by optimization of reaction parameters without leaving detrimental waste. This allows the adsorbent to be easily scaled and makes the preparation process rather environmentally friendly (Abou Taleb et al. 2008).

Several studies have reported the preparation of fibrous adsorbents by RIGC of GMA, which have an epoxy group allowing the amination of the grafted substrate with various amine groups (Abbasi et al.

2018, 2019b; Mohamad et al. 2021). However, the investigated fibrous CO_2 adsorbent have been mainly tested for adsorption of CO_2 from its mixtures with N_2 whereas their application in CO_2 capture from its mixtures with CH_4 have not been reported in the literature. Moreover, the adsorption isotherms, kinetics, and thermodynamics of adsorption on such aminated fibrous adsorbents have not been established. The objective of the present study is to investigate the CO_2 adsorption behaviour from CO_2/CH_4 mixtures on fibrous adsorbent immobilized with various amine groups hosted by poly (GMA) incorporated in PE/PP fibrous sheet by RIGC. The various properties of the adsorbents were evaluated. The performance was evaluated under various temperatures and pressures with different CO_2/CH_4 mixtures resembling the conditions of industrial removal of CO_2 from NG. Moreover, the adsorption isothermal, kinetic, and thermodynamic behaviours were studied by fitting the data to common models. The obtained fundamental properties such as adsorption capacity, kinetics, thermodynamics, and selectivity are essential for laying the foundation for process design parameters for CO_2 capture from NG with such fibrous adsorbents.

Experimental

Materials

The PE/PP fibrous sheet was obtained from Kurashiki Textile Manufacturing Co. Ltd. (Osaka, Japan). GMA monomer with 97% purity and polyoxyethylene sorbitol ester (Tween-20) were supplied by Sigma-Aldrich (Darmstadt, Germany). Ethylenediamine (EDA) (99% purity) and diethylenetriamine (DETA) (98% purity) were purchased from Merck Millipore (Darmstadt, Germany) and used without further treatment. Tetraethylenepentamine (TEPA) with purity of 95% was purchased from Acros Organics (California, United States). The isopropanol was purchased from Merck Millipore (Darmstadt, Germany). In all experiments, deionized water (DI) was obtained from a water purifier (Barnstead Nanopure Diamond Lab., ThermoFisher, Waltham, USA). The gases such as CO_2 (99.8% purity), helium (99.999% purity), and CH_4 (99.995% purity) were supplied by Alpha Gas Solution (Sdn Bhd, Malaysia).

Preparation of amine-functionalized fibrous adsorbent

The adsorbent was prepared in a two-step procedure started by RIGC of GMA onto pre-irradiated PE/PP fibrous sheet. The irradiation was performed by an electron beam (EB) accelerator (NHV-Nissin High Voltage, EPS3000) operated at an acceleration energy of 2 MeV and a beam current of 10 mA with a total dose of 50 kGy at 25 kGy/pass to create the free radicals. The irradiated PE/PP fibrous sheet was placed inside an ampoule containing an emulsion mixture comprising of 10% GMA in DI and containing 0.5% Tween 20 (surfactant) and bubbled with N_2 to remove O_2. The reaction was carried out at 50 ℃ for 35 minutes and yielded samples denoted as PE/PP-*g*-PGMA with 200% degree of grafting (DOG) which is calculated according to Eq. 1 (Zubair et al. 2020).

Degree of grafting (DG%) = $\frac{W_f - W_i}{W_i} \times 100$ (1)

where, W_i and W_f are the weights of the samples before and after grafting reaction, respectively. More details on preparation procedure can be found elsewhere (Nasef et al. 2014).

The grafted samples (PE/PP-*g*-PGMA) were functionalized by treatment with pure EDA or DETA. The reaction was conducted in a round bottom flask at 90 ºC under reflux and continuous stirring for 6 h. After reaction completion, the aminated sample was removed and repeatedly washed with DI water few times, then dried in a vacuum oven at 60 ºC for 5 h. On the other hand, the amination with TEPA amine was carried out by using 3:1 TEPA/isopropanol ratio and conducted at 83 ºC under reflux and continuous stirring for 4 h as previously reported (Mohamad et al. 2021). The weight changes of PE/PP-*g*-PGMA before and after the amination reaction were determined and used to calculate the percent of amination (A%) as Eq. 2.

$$\text{A (\%)} = \frac{(W_a - W_g)/MW}{(W_g - W_p)/142.15} \times 100 \quad (2)$$

where, W_p, W_g, and W_a are the weights of pristine, grafted, and aminated PE/PP substrates, respectively. MW is the molecular weight of amine group and 142.15 is the molecular weight of GMA. The final adsorbents are denoted as PE/PP-*g*-PGMA/EDA, PE/PP-*g*-PGMA/DETA, and PE/PP-*g*-PGMA/TEPA. All experiments were repeated 3 times, and the reported data for the A% is an average of 3 readings.

Properties of adsorbent

The changes in the chemical structure, morphology, thermal stability, crystallinity, and textural of the aminated fibrous adsorbent were evaluated and compared with both the pristine PE/PP and the grafted fibrous substrates. The changes in chemical composition were analysed using a Nicolet iS50 FT-IR spectrometer. The spectra were obtained with 32 scans and a resolution of 4 cm^{-1} across a frequency range of 500–4000 cm^{-1}. The morphological changes of the samples with respect to fibre diameter were examined using a GEMINISEM 500 microscope. The thermal stability of the samples was tested using a Q50 thermogravimetric analyser (TA Instruments) at a heating rate of 10 ^{o}C/min in a temperature range of 30–700 ^{o}C. The crystalline structure of the samples was examined by X-ray diffraction (XRD) using a PANalytical Empyrean analyser at Bragg's angle in the range of 5–70°. BET test was performed with Quantachrome Instrument (Novatouch) to measure surface area and pore analysis. The samples were degassed at 80°C for 4 h before analysis.

Gas adsorption measurements

The CO_2 adsorption capacity measurements were carried out using the magnetic suspension balance (MSB) known as isoSORP® gravimetric analyser manufactured by RUBOTHERM (Bochum, Germany). Details of MSB's basic principles, components, and operational procedure were described elsewhere (Fujii et al. 2010; Schell et al. 2012). One cycle of adsorption measurement consists of three steps comprising pre-treatment, buoyancy, and adsorption measurement. All the data were recorded by RUBOTHERM control system software (RSCS-2016). The adsorbent sample was subjected to a pre-treatment started by heating the samples at 80 ^{o}C for 4.5 h under vacuum until the recorded weight loss reached a constant to

eliminate any retained moisture. Subsequently, the buoyancy measurement was carried out to precisely determine the weight and volume of adsorbent sample using purified helium gas at the required sorption temperature under varying pressure from vacuum condition to 30 bar. Finally, the adsorption measurements of pure gases (CO_2 and CH_4) and their gas mixture at different ratios (20–80% CO_2/CH_4) and different operating conditions, including different pressures up to 30 bar were carried out at. The equilibrium sorption was achieved in about 50 minutes for each pressure reading.

CO_2/CH_4 selectivity

The ideal selectivity (S) of CO_2 over CH_4 was estimated using adsorption capacity data of pure gases using the following equation (Mukhtar et al. 2020a):

$$S_{CO_2/CH_4} = \left(\frac{q_{CO_2}}{q_{CH_4}}\right) \times \left(\frac{P_{CH_4}}{P_{CO_2}}\right)$$

3

where, *q* is the adsorption capacity (mmol/g), and *P* is the operating pressure (bar), respectively.

kinetics adsorption on fibrous adsorbent

Few kinetic models were proposed to describe the kinetic behaviour of adsorption on solid adsorbents. The kinetic models that were tested in this work include the following (Rahafza et al. 2018):

i. Pseudo-first-order kinetic model

The non-linear form of this model is expressed in the following equation:

$$q_t = q_e(1 - e^{-k_1 \mathrm{t}})$$

4

where, q_t and q_e are the amounts (mmol/g) of the adsorbate adsorbed at time "*t*" (min), and at an equilibrium, respectively. k_1 is the pseudo first order rate constant (1/min).

ii. Pseudo-second-order kinetic model

The non-linear form of pseudo second order equation is given by Eq. 5:

$$q_t = \frac{q_e^2 k_2 t}{1 + q_e k_2 t}$$

5

where, k_2 is the rate constant of pseudo second order model (mol/g.min)

iii. Elovich kinetic model

The Elovich kinetic model is expressed as follows:

$$q_t = \frac{1}{\beta}\ln(\alpha\beta t + 1)$$

6

where, α is the initial adsorption rate and β is the desorption constant during each experiment.

Adsorption isotherms for CO_2 adsorption on fibrous adsorbent

Adsorption isotherms at equilibrium are used to describe the interaction between the adsorbent and targeted adsorbate. The equilibrium isotherm data provides significant explanations and information on the surface properties and mechanisms of the adsorption process. The fitting of adsorption isotherm data to an adsorption isotherm model is crucial in determining the model representing the experimental data for design purposes (Raganati et al. 2018). The adsorption isotherm models are described as follows:

Langmuir isotherm

According to the Langmuir theory, only one adsorbate (CO_2) molecule can bind to each active site on the adsorbent surface, explaining the monolayer adsorption process. The non-linear form of the Langmuir isotherm model equation is as follow

$$q_e = \frac{K_L P q_m}{1 + K_L P}$$

7

where, q_e(mmol/g) is the adsorbed amount of CO_2, P is the pressure (bar), q_m (mmol/g) is the maximum monolayer adsorption capacity and K_L is the Langmuir equilibrium constant related to adsorption capacity and adsorption intensity.

Freundlich isotherm

Freundlich isotherm model accounts for a heterogonous adsorption system. This isotherm can be used to define the multilayer uptake of CO_2 molecules adsorbed onto the adsorbent surface. The non-linear form of Freundlich isotherm model equation is expressed as follows

$$q_e = K_f P^{1/n} \quad (8)$$

where, K_f is the Freundlich constant, while n is the factor of heterogeneity, which related to the adsorbate affinity to the adsorbent.

Sips isotherm

Sips isotherm model indicates that the adsorption process of CO_2 molecules onto the adsorbent surface follows a combination of Langmuir and Freundlich isotherm models. The non-linear equation of Sips isotherm model is expressed as follows

$$q_e = \frac{q_s K_s P^s}{1 + K_s P^s}$$

9

where, q_s is the Sips isotherm maximum adsorption capacity, K_s is the Sips isotherm constant, and *s* is the Sips exponent. If *s* equals to 1, it represents a homogeneous system.

Thermodynamics of adsorption on fibrous adsorbent

Thermodynamic properties are crucial in the adsorption process to determine the spontaneity of the reaction between the adsorbent and adsorbate. Besides, the nature of adsorption including physisorption or chemisorption can be determine through the evaluation of the thermodynamic properties such as standard Gibbs free energy change (ΔG°), the enthalpy change (ΔH°), and the entropy change (ΔS°) by using Eq. 10 (Raganati et al. 2018). For instance, physisorption arises from relatively weak interactions such as van der Waals force, while chemisorption involves a stronger chemical interaction (covalent bonding). The ΔG° can be directly calculated from Eq. 11 once the thermodynamic constant is obtained. The thermodynamic constant can be derived from various isothermal model types, including Langmuir, Freundlich, Sips, and others (Tran et al. 2016). The enthalpy change (ΔH°), also known as heat of adsorption and the entropy change ΔS° corresponds to the slope and intercept from van't Hoff plot correlating ln Ks with 1/T and calculated using Eq. 12.

$\Delta G° = \Delta H° - T\Delta S°$ (10)

$\Delta G° = -RT \ln K_S$ (11)

$\ln K_S = (\frac{\Delta S^\circ}{R}) - (\frac{\Delta H^\circ}{RT})$ (12)

where, T is the temperature (K), R is the universal gas constant (J/mol.K) and K_S is the thermodynamic constant.

Results And Discussions

Amine-containing adsorbents

Preparation of the adsorbents was carried out in a 2-step procedure (grafting of GMA and immobilization of amine). Both grafting and amination parameters were selected based on our previous investigation (Mohamad et al. 2021) and yielded samples with DG of 200% and amination percent (A%) in the range of 70–80% (A%) was obtained in all aminated samples. The preparation of the adsorbent by grafting of GMA and amination with TEPA is illustrated in the schematic diagram shown in Fig. 1.

Properties of adsorbent with different amines

Chemical composition properties

Figure 2 shows the FTIR spectra of pristine PE/PP sheet, PGMA grafted PE/PP sheet, and PE/PP-*g*-PGMA sheets aminated with EDA, DETA, and TEPA. It can be observed that the representative diagnostic peaks at 2917 and 2847 cm^{-1} corresponding to the antisymmetric and asymmetric stretching vibration of C-H coming from PE/PP backbone, respectively. The peaks appeared at 1740 and 1255 cm^{-1} are attributed to group (-COC) originated from epoxide ring of PGMA formed after grafting, and remained in a weaken form after amination (Abbasi et al. 2019a). In addition, the incorporation of PGMA to the PE/PP structure was also proved by the emergence of two bands at 905 and 840 cm^{-1}, which are assigned for -CO of the epoxy group (Nasef et al. 2014). The evidence of -NH absorptions originating from the primary amine and secondary amine functionalization appeared in the peaks at around 1527 and 1658 cm^{-1}, respectively (Ullah et al. 2015). The peak at 1156 cm^{-1} represents the -CN stretching vibration in TEPA. It can be concluded that the obtained adsorbent composed of PE/PP sheets containing PGMA side chain graft immobilized with amines.

Morphological Properties

The SEM images of pristine PE/PP, PE/PP-*g*-PGMA, PE/PP-*g*-PGMA/EDA, PE/PP-*g*-PGMA/DETA, and PE/PP-*g*-PGMA/TEPA sheets are presented in Fig. 3. The images revealed that there are changes in the average fibre diameter (AFD) in the sheets after grafting and amine functionalization. For instance, the AFD of the pristine PE/PP was 15.3 ± 3.18 µm, which increased after grafting with PGMA to 20.0 ± 5.70 µm. Such an increase in AFD is coming from the covalent incorporation of PGMA around the fibres and similar trend was reported for grafting of vinyl monomers on fibrous substrates (Othman et al. 2019). On the other hand, amination with EDA and DETA led to a reduction in the average fibre diameter by ~ 7.4% to reach values of 18.50 ± 5.6. This is likely due to minor degradation of tiny amount of unbound PGMA side chains caused by using of concentrated amine agents. However, the AFD was increased to 24.18 ± 6.20 µm after amination with TEPA diluted in isopropanol. These results provide further evidence for grafting of GMA and subsequent amination with EDA, DETA and TEPA of PE/PP fibrous sheet.

Thermal Properties

Figure 4 shows TGA thermograms of pristine PE/PP, PE/PP-*g*-PGMA, and PE/PP-*g*-PGMA/EDA (-DETA and -TEPA) sheets. A single step degradation was observed in the thermogram of the pristine PE/PP sample at temperature 350°C due to the principal polymeric backbone thermal decomposition (Abbasi et al. 2019a). The PE/PP-*g*-PGMA sample shows a two-step degradation pattern 200°C and 350°C coming from the decomposition of PGMA and PE/PP backbone (Xu et al. 2015). The aminated samples showed multiple degradation pattern represented by weight loss at 4 different temperature regions. The first weight loss started below 100°C and continued to 150°C is due to the removal of moisture bound to the amine groups bound by hydrogen bonds (Choi et al. 2001). The continuous of weight loss at ~ 200°C is due to the decomposition of amine (Mohamad et al. 2021). The weight loss coming from the

deterioration of the grafted PGMA appeared at 250°C and that due decomposition of PE/PP backbone was at 350°C.

Crystalline structure properties

Figure 5 shows X-ray diffractograms of pristine PE/PP, grafted PE/PP-*g*-PGMA, and all three different types of amine-functionalized PE/PP-*g*-PGMA. The crystalline peaks in all diffractograms showed no changes in Bragg's angles regardless the of the type of immobilized amine suggesting that the backbone structure of PE/PP is well preserved and remain intact even after grafting and subsequent amination. It is confirmed that PGMA and all three types of amine have no contribution to the diffraction pattern (Nasef et al. 1998). However, the degree of crystallinity decreased after grafting and even more after the amination. For instance, the intensity of the crystalline peaks decreased in a sequence of pristine PE/PP > PE/PP-*g*-PGMA > PE/PP-*g*-PGMA/EDA > PE/PP-*g*-PGMA/TEPA > PE/PP-*g*-PGMA/DETA. This reduction in the peak intensity is due to the dilution of the inherent crystallinity by incorporating amorphous PGMA, and such effect became more profound after immobilization of amines with PE/PP-*g*-PGMA/DETA showing the lowest degree of crystallinity (Sharif et al. 2013). These results suggest that the aminated adsorbents retained reasonable physical integrity suitable for adsorption applications.

Surface area and pore analysis

The nitrogen adsorption-desorption isotherm was evaluated using BET analysis to determine the surface area, pore volume and pore width of PGMA grafted and amine functionalized substrate which tabulated in Table 1. It can be seen that the surface area was obtained for PE/PP-*g*-PGMA, PE/PP-*g*-PGMA/EDA, PE/PP-*g*-PGMA/DETA, and PE/PP-*g*-PGMA/TEPA fibrous sheets, where surface areas of 7.50, 5.46, 5.38, and 3.47 $m^2\ g^{-1}$ were observed, respectively. After functionalization with amine, the surface area decreased, and such a decrease was higher with longer aliphatic chain of the amine. The immobilization of amines to the grafted fibrous sheet not only makes the amine dominate the pore and reduces the surface area but also lowers the pore volume value. These results emphasize that surface area which is small in these adsorbents is not the crucial factor in the adsorption mechanism and it is the number of amine sites and their accessibility that will dominate the performance of these fibrous adsorbents.

Table 1
Surface area and pore properties of PE/PP-*g*-PGMA, PE/PP-*g*-PGMA/EDA, PE/PP-*g*-PGMA/DETA and PE/PP-*g*-PGMA/TEPA fibrous sheets

Samples	Surface area ($m^2\ g^{-1}$)	Pore width (nm)	Pore volume $x10^{-3}$ ($cm^3\ g^{-1}$)
PE/PP-*g*-PGMA	7.50	5.89	7.97
PE/PP-*g*-PGMA/EDA	5.46	2.44	4.66
PE/PP-*g*-PGMA/DETA	5.38	1.91	4.61
PE/PP-*g*-PGMA/TEPA	3.47	2.30	4.11

Effect of amine types on the CO_2 adsorption

The adsorption capacity of pure CO_2 was measured at different pressures (up to 30 bar) for PE/PP-*g*-PGMA/EDA, PE/PP-*g*-PGMA/DETA, and PE/PP-*g*-PGMA/TEPA at room temperature and the obtained adsorption data is presented in Fig. 6. The CO_2 adsorption capacity increased gradually with the increase in the pressure for all adsorbents without reaching saturation suggesting a trend close to type II adsorption isotherms (nonporous adsorbent) and the presence of a combination monolayer and multilayer adsorptions on the present adsorbent. The continuous increasing trend in CO_2 adsorption capacity can be attributed to the early interaction with energetic amine at the surface followed by the successive diffusion of CO_2 to the inner layers reaching deeper amine sites under the influence of the pressure increase (Ahmed et al. 2017).

The CO_2 adsorption capacity was in the following order: PE/PP-*g*-PGMA/TEPA > PE/PP-*g*-PGMA/DETA > PE/PP-*g*-PGMA/EDA, with the values of 2.12 mmol/g > 1.49 mmol/g > 1.21 mmol/g. This trend could be because the secondary amine is more efficient than the primary amine at interacting with CO_2 molecules (Liu et al. 2017). Therefore, the superior CO_2 adsorption of PE/PP-*g*-PGMA/TEPA adsorbent is attributable to larger number secondary amine groups in TEPA compared to DETA and EDA. Thus, PE/PP-*g*-PGMA/TEPA is selected to further investigate the adsorption behavior of CO_2 under various temperatures.

Effect of temperature on CO_2 adsorption on TEPA-containing adsorbent

Figure 7 shows the variation of pure CO_2 gas adsorption with the temperature in the range of 30–70°C at 30 bar. It can be observed that the rise in the temperature leads to an increase in the adsorption capacity until 60°C beyond which it declines. For instance, the CO_2 adsorption capacity reached a maximum value of 2.66 mmol/g at 60°C and slipped to 2.62 mmol/g at 70°C. The increased CO_2 adsorption capacity with the temperature rise is not only due to enhancement of CO_2 diffusion rate and the increase in the CO_2 molecules kinetic energy but also to the acceleration in CO_2 accessibility to the inner layers containing more TEPA sites (Zhao et al. 2022). Thus, the increase in adsorption capacity with temperature up to 60°C indicates that the CO_2 capture process is controlled by kinetic rather than thermodynamic factors (Zhao et al. 2017). The observation of increasing adsorption with temperature suggests that the CO_2 adsorption on the present fibrous adsorbent does not follow the Clausius-Clapeyron equation (Yano et al. 2020). Similar deviation from adsorption thermodynamics was also report in literature for TEPA modified carbon nanotubes [48] and mesoporous carbon [49]. It can be concluded that 60°C is the best temperature for the maximum adsorption capacity which makes this adsorbent favourable for CO_2 capture from NG as the commercial technology of amine absorption typically operate at 50 to 60°C.

Adsorption of pure CO_2 and CH_4 on PE/PP-g-PGMA/TEPA adsorbent

Figure 8a shows the adsorption behaviour of pure CO_2 and CH_4 gases on PE/PP-*g*-PGMA/TEPA adsorbent at different pressures and temperatures. It can be seen that the higher pressures and

temperatures (30–60°C) led to higher CO_2 adsorption performance unlike CH_4 which showed very tiny adsorption (0.02–0.04 mmol/g), which seems to be insignificant at all temperatures and pressures. This observation suggests that PE/PP-*g*-PGMA/TEPA adsorbent has high CO_2 selectivity over CH_4.

The CO_2/CH_4 ideal selectivity for PE/PP-*g*-PGMA/TEPA was evaluated and presented in correlation with pressures at different temperatures in Fig. 8b. As the pressure increases, the CO_2/CH_4 selectivity decreased for all temperatures, which can be attributed to the pressure-driven mechanism through amine containing sites in different layers irrespective to those bound to the surface of the adsorbent (Mukhtar et al. 2020a, b). Overall, the CO_2/CH_4 selectivity for all pressure readings is considered high where all of them are above value of 50, showing superior CO_2 adsorption compared to CH_4, which is far better than those reported in the previous studies (Vosoughi et al. 2021) (Zohdi et al. 2019). Therefore, it can be suggested that TEPA-aminated adsorbent has a strong potential for separating CO_2 from it mixtures with CH_4 (Dao et al. 2020). This information is crucial for the development of NG treatment technologies since CO_2 capture from NG demands designing highly CO_2 selective adsorbent material (Mukhtar et al. 2020a).

Adsorption of CO_2 from CO_2/CH_4 mixtures

The effect of variation of CO_2/CH_4 gas mixture composition and pressure on the adsorption capacity of CO_2 on PE/PP-*g*-PGMA/TEPA adsorbent is presented in Fig. 9. Pure CO_2 and CH_4 adsorption variation with the same pressure range were used as references. The CO_2 adsorption capacity increased with the rise in the pressure and CO_2 composition. The adsorption capacity was found to be in the following sequence at 30 bar: 100% CH_4 < 20%CO_2 < 40%CO_2 < 60%CO_2 < 80%CO_2 < 100% CO_2 with their adsorption capacity were 0.02, 1.50, 2.00, 2.30, 2.57, and 2.66 mmol/g, respectively. The decrease of the adsorption capacity with the CO_2 lessening in the feed mixture is most likely caused by accumulation of the CH_4 around TEPA aminated sites reducing their accessibility by CO_2. This is going along with the fact that, CH_4 has lighter molecular weight (16.04 g/mol) than CO_2 (44.01 g/mol), leading to higher rate of diffusion, which is inversely proportional to the square root of its molecular mass as per Graham's law of diffusion (Rani et al. 2018). Thus, the CO_2 access to TEPA groups in the adsorbent is hindered. This observation suggests that the present adsorbent works best at high CO_2 concentrations in the feed and is likely to be useful for purification of NG with high CO_2 concentration.

Adsorption/desorption cyclic stability

The effect of number of adsorption/desorption cycles on the adsorption capacity of pure CO_2 on PE/PP-*g*-PGMA/TEPA adsorbent is evaluated in ten cycles, and the obtained data is presented in Fig. 10. As can be clearly seen, the CO_2 adsorption capacity remained almost unvaried at the value of 2.66 mmol/g (the adsorption capacity of the first cycle is 2.65 mmol/g). The absence of any significant adsorption capacity loss confirms the high stability of the present adsorbent and it suitability for prolonged cyclic operation.

Comparison of kinetic models

Three models including pseudo-first-order, pseudo-second-order, and Elovich kinetic models were used to fit the experimental CO_2 adsorption results. The data are presented in Table 2 and plotted in Fig. 11. The experimental data was found to best fit the Elovich kinetic model with the coefficient of determination (R^2) values are the highest associated with lowest standard error (SE) values at all temperatures (30, 40, 50, and 60°C) compared to pseudo second-order and pseudo-first-order kinetic models both which indicate that the CO_2 adsorption rate of the adsorbent for capture is controlled by surface diffusion and chemical reactions at the gas-solid interface. The results best fitting of data to Elovich kinetic models suggests that the CO_2 adsorption process in the present system occurs as a group of reactions including surface diffusion, bulk phase diffusion, and active ionic surfaces. It also describes the chemisorption process in relation to the amount of surface coverage and decrease in the adsorption rate (Najafi et al. 2021). The reaction rate of CO_2 adsorption was enhanced as the β value was found to increase with the rise in the adsorption temperature from 30 to 60°C (Rahafza et al. 2018).

Table 2
Comparison of parameters of the kinetic models at 30, 40, 50, and 60°C

Temperature (°C)		30	40	50	60
Pseudo-first-order	q (mmol/g)	2.41	2.40	2.68	2.53
	k_1	0.0068	0.0073	0.0079	0.0125
	R^2	0.9448	0.9269	0.8677	0.8613
	SE	0.014	0.019	0.044	0.044
Pseudo-second-order	q (mmol/g)	3.42	3.37	3.51	3.13
	k_2	0.0016	0.0018	0.0021	0.0044
	R^2	0.9532	0.9377	0.8914	0.9044
	SE	0.012	0.016	0.0360	0.031
Elovich	α	0.0220	0.0244	0.0371	0.0733
	β	0.9185	0.9529	1.0430	1.3165
	k_E	0.0240	0.0256	0.0356	0.0557
	R^2	0.9616	0.9493	0.9173	0.9440
	SE	0.010	0.0130	0.0270	0.0180

Adsorption isotherms for CO_2 adsorption on PE/PP-g-PGMA/TEPA

Figure 12 shows the adsorption isotherms and curve fitting for CO_2 adsorption on PE/PP-*g*-PGMA/TEPA at different temperatures using various isothermal models such as Langmuir, Freundlich, and Sips whereas, the relevant parametric data is presented in Table 3. To avoid inaccuracy from linearization, the magnitude of adsorption isotherm parameters in this study were obtained using the non-linear regression analysis. It can be seen that the highest value of R^2 with more than 0.99 and the lowest value of SE for Sips isotherm model among others for all operating temperatures indicating that the adsorption process of CO_2 molecules on the PE/PP-*g*-PGMA/TEPA adsorbent surface follows Sips isotherm model. This suggests the presence of monolayer and multilayer adsorption. Lastly, the value of Sips constant, K_s was increased with the temperature increase. This demonstrated that the binding affinity of CO_2

molecules with the fibrous surface of PE/PP-*g*-PGMA/TEPA becomes more vital with the rise of temperature up to 60°C.

Table 3
Data of isothermal models for CO_2 adsorption on PE/PP-*g*-PGMA/TEPA at different temperatures

Models	Parameters	Temperature (°C)			
		30	40	50	60
Langmuir	K_L	0.0446	0.1124	0.1602	0.2208
	q_m	3.6465	2.6790	3.0758	2.9949
	R^2	0.9948	0.9960	0.9952	0.9974
	SE	0.338	0.252	0.463	0.258
Freundlich	K_f	0.2869	0.5536	0.6899	0.8350
	n	1.6943	2.5227	3.0628	3.7313
	1/n	0.5902	0.3964	0.3265	0.2680
	R^2	0.9933	0.9988	0.9989	0.9968
	SE	0.225	0.023	0.024	0.058
Sips	K_s	0.0187	0.0690	0.0734	0.2273
	q_s	14.2585	7.7370	11.9479	4.9532
	s	0.6574	0.4996	0.3943	0.4787
	R^2	0.9973	0.9998	0.9998	0.9999
	SE	0.217	0.009	0.016	0.003

Figure 13 shows Van't Hoff plot for adsorption CO_2 on PE/PP-*g*-PGMA/TEPA adsorbent in which lnK_S was plotted versus *1/T*. The K_S in Eq. 12, which is the thermodynamic constant was obtained from the Sips isotherm model fitting parameters reported in Table 3. To further investigate the effect of thermodynamics on the CO_2 adsorption on PE/PP-*g*-PGMA/TEPA adsorbent and understand the mechanism of adsorption. The thermodynamic parameters for the CO_2 adsorption onto PE/PP-*g*-

PGMA/TEPA adsorbent were studied and the obtained data are presented in Table 4. The intercept and slope from Van't Hoff plot were used in equations 10–12 to calculate ΔG°, ΔH° and ΔS°, respectively. The value of ΔG° is positive at each temperature. This indicates that the adsorption process is not thermodynamically favourable, non-spontaneous and needs energy to initiate the reaction between the adsorbent and adsorbate. Moreover, there is a decreasing value of ΔG° with temperature rise as depicted in Table 4 and this suggests that the adsorption process is decreasing in the non-spontaneity and it becomes more favourable at higher temperatures (up to 60°C) as the energy needed to promote the adsorption reaction (Mukhtar et al. 2020a). A positive value of ΔH° was obtained in this study shows an endothermic nature of the adsorption process, which reflects the increasing temperature that caused an increased adsorption capacity as presented in Fig. 7. The endothermic adsorption process (ΔH° > 0) suggests that adsorption of CO_2 is associated with energy adsorption in the form of heat from the surrounding. This endothermic phenomenon is mostly because the total energy absorbed in bond breaking is higher than that released in the bond making between CO_2 and adsorbent (Tran et al. 2016). Furthermore, ΔH° value also provides a clear understanding of the adsorption mechanism. Theoretically, ΔH° < 20 kJ/mol is for the physisorption process and ΔH° > 80 kJ/mol is for the chemisorption process (Raganati et al. 2018). Hence, 63.44 kJ/mol of ΔH° obtained in this study confirmed the presence of chemisorption interaction between the CO_2 molecules and PE/PP-*g*-PGMA/TEPA adsorbent. These results are in a complete agreement with the study from Qi *et al* (Qi et al. 2021) who obtained a positive value of ΔH° for all samples that were functionalized with TEPA. Yang *et al* and Shi *et al* (Shi et al. 2021; HaiyanYang et al. 2022) reported similar adsorption behaviour and claimed the reaction between TEPA and CO_2 is an endothermic chemical reaction. In the meantime, the entropy (ΔS°) was used to determine the randomness of the adsorption process. A positive ΔS° value of 0.18 kJ/mol was obtained prevailing a typical chemisorption and suggesting not only an increase in the randomness at the solid-gas interface during the adsorption process but also the presence of a good affinity between the CO_2 molecules and PE/PP-*g*-PGMA/TEPA adsorbent surface (Ebelegi et al. 2020; Edet and Ifelebuegu 2020).

Table 4
Thermodynamic properties for CO_2 adsorption on PE/PP-*g*-PGMA/TEPA adsorbent

ΔH° (KJ/mol)	ΔS°(KJ/mol)	ΔG°(KJ/mol)			
63.44	0.18	30°C	40°C	50°C	60°C
		10.02	6.74	6.58	3.73

Conclusion

Amine-containing adsorbents with fibrous structures were prepared, characterized, and tested for adsorption of CO_2 and separation of mixtures of CO_2/CH_4. The adsorbent was prepared by grafting of GMA onto EB irradiated PP/PE fibrous sheets followed by immobilization of desired amine group under controlled conditions. The covalent grafting of aminated side chains was verified and the morphology as

well as the structure and thermal stability were proven. The PE/PP-*g*-PGMA/TEPA adsorbent with highest number of secondary amine groups demonstrated a maximum CO_2 adsorption capacity (2.12 mmol/g) compared to those loaded with DETA and EDA. The increase in the pressure up to 30 bar led to an increase in the adsorption capacity, which was also increased with the rise in the temperature up 60°C to a value of 2.66 mmol/g beyond which it declined. This suggested that the CO_2 capture process is controlled by kinetics rather than thermodynamic factors. The adsorbent demonstrated a high stability during ten adsorption-desorption cycles at relatively low regeneration temperature of 80°C. The CO_2 adsorption isotherm was best represented by Sips model suggesting the presence of monolayer and multilayer adsorption in the TEPA containing adsorbent. The adsorption kinetics data was found to best fit Elovich model indicating that adsorption mainly proceeds by chemisorption mechanism involving steps such as surface diffusion, bulk phase diffusion, and active ionic interaction. The thermodynamic properties revealed that the adsorption process is non-spontaneous and endothermic in nature. Finally, the high CO_2 selectivity shown by the adsorbent towards CO_2 signify its potential for separating CO_2 from its mixtures with CH_4 especially at high CO_2 concentrations in the feed. Thus, this adsorbent is likely to be promising for purification of NG with high CO_2 concentrations.

Declarations

Funding

This work was supported by Malaysia Thailand Joint Authority (MTJA) under grant no # R.J130000.7609.4C172 and International Atomic Energy Agency (IAEA) under coordinated research projects (CRP) no # F22072 with grant no # R.K130000.7343.4B623.

Author contributions: The work is conceptualized and supervised by M.M. Nasef and A. Ahmad. Materials' preparation and data collection were performed by N. A. Mohamad and T.M. Ting. Data analysis was carried out by N. A. Mohamad and M. M. Nasef. Writing, revision, and editing: Noor N. A. Mohamad and M. M. Nasef, T. A. T. Abdullah, A. Ahmad and T. M. Ting. All authors have reviewed and approved the final version of the manuscript prior to submission.

Data availability All data used to support the findings of this study are included in the article.

Ethics approval and consent to participate Not applicable.

Consent for publication Not applicable.

Competing interests The authors declare no competing onterests.

References

1. Abbasi A, Nasef MM, Babadi FE, et al (2019a) Carbon Dioxide Adsorption on Grafted Nanofibrous Adsorbents Functionalized Using Different Amines. Front Energy Res 7:1–14.

https://doi.org/10.3389/fenrg.2019.00145

2. Abbasi A, Nasef MM, Faridi-Majidi R, et al (2018) Highly flexible method for fabrication of poly (Glycidyl Methacrylate) grafted polyolefin nanofiber. Radiat Phys Chem 151:283–291. https://doi.org/10.1016/j.radphyschem.2018.07.002
3. Abbasi A, Nasef MM, Kheawhom S, et al (2019b) Amine functionalized radiation induced grafted polyole fi n nano fi bers for CO 2 adsorption. Radiat Phys Chem 156:58–66. https://doi.org/10.1016/j.radphyschem.2018.10.015
4. Abid HR, Pham GH, Ang HM, et al (2012) Adsorption of CH4 and CO2 on Zr-metal organic frameworks. J Colloid Interface Sci 366:120–124. https://doi.org/10.1016/j.jcis.2011.09.060
5. Abou Taleb MF, Mahmoud GA, Elsigeny SM, Hegazy ESA (2008) Adsorption and desorption of phosphate and nitrate ions using quaternary (polypropylene-g-N,N-dimethylamino ethylmethacrylate) graft copolymer. J Hazard Mater 159:372–379. https://doi.org/10.1016/j.jhazmat.2008.02.028
6. Adewole JK, Ahmad AL, Ismail S, Leo CP (2013) Current challenges in membrane separation of CO2 from natural gas: A review. Int J Greenh Gas Control 17:46–65. https://doi.org/10.1016/j.ijggc.2013.04.012
7. Ahmed S, Ramli A, Yusup S (2017) Development of polyethylenimine-functionalized mesoporous Si-MCM-41 for CO2 adsorption. Fuel Process Technol 167:622–630. https://doi.org/10.1016/j.fuproc.2017.07.036
8. Attia NF, Jung M, Park J, et al (2020) Flexible nanoporous activated carbon cloth for achieving high H2, CH4, and CO2 storage capacities and selective CO2/CH4 separation. Chem Eng J 379:122367. https://doi.org/10.1016/j.cej.2019.122367
9. Chen S, Tian M, Tao Z, et al (2020) Effect of swing on removing CO2 from offshore natural gas by adsorption. Chem Eng J 382:. https://doi.org/10.1016/j.cej.2019.122932
10. Chen SJ, Tao ZC, Fu Y, et al (2017) CO2 separation from offshore natural gas in quiescent and flowing states using 13X zeolite. Appl Energy 205:1435–1446. https://doi.org/10.1016/j.apenergy.2017.09.084
11. Choi SH, Lee KP, Nho YC (2001) Adsorption of urokinase by polypropylene films with various amine groups. J Appl Polym Sci 80:2851–2858. https://doi.org/10.1002/app.1402
12. Danaci D, Singh R, Xiao P, Webley PA (2015) Assessment of ZIF materials for CO2 capture from high pressure natural gas streams. Chem Eng J 280:486–493. https://doi.org/10.1016/j.cej.2015.04.090
13. Dao DS, Yamada H, Yogo K (2020) Enhancement of CO2Adsorption/Desorption Properties of Solid Sorbents Using Tetraethylenepentamine/Diethanolamine Blends. ACS Omega 5:23533–23541. https://doi.org/10.1021/acsomega.0c01515
14. Ebelegi AN, Ayawei N, Wankasi D (2020) Interpretation of Adsorption Thermodynamics and Kinetics. Open J Phys Chem 10:166–182. https://doi.org/10.4236/ojpc.2020.103010
15. Edet UA, Ifelebuegu AO (2020) Kinetics, isotherms, and thermodynamic modeling of the adsorption of phosphates from model wastewater using recycled brick waste. Processes 8:. https://doi.org/10.3390/PR8060665

16. Fujii T, Nakagawa S, Sato Y, et al (2010) Sorption Characteristics of CO2 on Rocks and Minerals in Storing CO2 Processes. Nat Resour 01:1–10. https://doi.org/10.4236/nr.2010.11001
17. Furukawa H, Go YB, Aratani N, et al (2010) Ultrahigh porosity in metal-organic frameworks. Science (80-) 329:424–428. https://doi.org/10.1126/science.1192160
18. HaiyanYang, Wang X, Liu J, et al (2022) Amine-impregnated polymeric resin with high CO2 adsorption capacity for biogas upgrading. Chem Eng J 430:132899. https://doi.org/10.1016/j.cej.2021.132899
19. Han Y, Ho WSW (2021) Polymeric membranes for CO2 separation and capture. J Memb Sci 628:119244. https://doi.org/10.1016/j.memsci.2021.119244
20. Imanian Z, Hormozi F, Torab-Mostaedi M, Asadollahzadeh M (2022) Highly selective adsorbent by gamma radiation-induced grafting of glycidyl methacrylate on polyacrylonitrile/polyurethane nanofiber: Evaluation of CO2 capture. Sep Purif Technol 289:120749. https://doi.org/10.1016/j.seppur.2022.120749
21. Kavaklı C, Barsbay M, Tilki S, et al (2016) Activation of Polyethylene/Polypropylene Nonwoven Fabric by Radiation-Induced Grafting for the Removal of Cr(VI) from Aqueous Solutions. Water Air Soil Pollut 227:. https://doi.org/10.1007/s11270-016-3184-5
22. Lee SP, Mellon N, Shariff AM, Leveque JM (2018) High-pressure CO2-CH4 selective adsorption on covalent organic polymer. J Nat Gas Sci Eng 50:139–146. https://doi.org/10.1016/j.jngse.2017.11.024
23. Liu F, Chen S, Gao Y, Xie Y (2017) Synthesis and CO2 adsorption behavior of amine-functionalized porous polystyrene adsorbent. J Appl Polym Sci 134:1–7. https://doi.org/10.1002/app.45046
24. Mallick A, Mouchaham G, Bhatt PM, et al (2018) Advances in Shaping of Metal-Organic Frameworks for CO2 Capture: Understanding the Effect of Rubbery and Glassy Polymeric Binders. Ind Eng Chem Res 57:16897–16902. https://doi.org/10.1021/acs.iecr.8b03937
25. Mohamad NA, Nasef MM, Nia PM, et al (2021) Tetraethylenepentamine-containing adsorbent with optimized amination efficiency based on grafted polyolefin microfibrous substrate for CO2 adsorption. Arab J Chem 14:103067. https://doi.org/10.1016/j.arabjc.2021.103067
26. Mukhtar A, Mellon N, Saqib S, et al (2020a) CO2/CH4 adsorption over functionalized multi-walled carbon nanotubes; an experimental study, isotherms analysis, mechanism, and thermodynamics. Microporous Mesoporous Mater 294:109883. https://doi.org/10.1016/j.micromeso.2019.109883
27. Mukhtar A, Mellon NB, Bustam MA, et al (2020b) Impact of amine functionality on the selective CO2/CH4 adsorption behavior of porous covalent triazine adsorbent. J Nat Gas Sci Eng 83:103582. https://doi.org/10.1016/j.jngse.2020.103582
28. Mukhtar A, Saqib S, Mellon NB, et al (2020c) CO2 capturing, thermo-kinetic principles, synthesis and amine functionalization of covalent organic polymers for CO2 separation from natural gas: A review. J Nat Gas Sci Eng 77:103203. https://doi.org/10.1016/j.jngse.2020.103203
29. Najafı P, Ramezanipour H, Ghaemi A (2021) Environmental Technology & Innovation Synthesis and characterization of Benzyl chloride-based hypercrosslinked polymers and its amine-modification as

an adsorbent for CO 2 capture. Environ Technol Innov 23:101746. https://doi.org/10.1016/j.eti.2021.101746

30. Nasef MM, Abbasi A, Ting TM (2014) New CO2 adsorbent containing aminated poly(glycidyl methacrylate) grafted onto irradiated PE-PP nonwoven sheet. Radiat Phys Chem 103:72–74. https://doi.org/10.1016/j.radphyschem.2014.05.031
31. Nasef MM, Güven O (2012) Radiation-grafted copolymers for separation and purification purposes: Status, challenges and future directions. Prog Polym Sci 37:1597–1656. https://doi.org/10.1016/j.progpolymsci.2012.07.004
32. Nasef MM, Saidi H, Mohd Nor H, et al (1998) Cation Exchange Membranes by Radiation-Induced Graft Copolymerization of Styrene onto PFA Copolymer Films . I . Preparation and Characterization of the Graft Copolymer. J Appl Polym Sci 73:2095–2102
33. Othman NAF, Selambakkannu S, Abdullah TAT, et al (2019) Selectivity of copper by amine-based ion recognition polymer adsorbent with different aliphatic amines. Polymers (Basel) 11:. https://doi.org/10.3390/polym11121994
34. Petrovic B, Gorbounov M, Masoudi Soltani S (2021) Influence of surface modification on selective CO2 adsorption: A technical review on mechanisms and methods. Microporous Mesoporous Mater 312:110751. https://doi.org/10.1016/j.micromeso.2020.110751
35. Qi L, Han Y, Bai G, et al (2021) Role of Brush-like Additives in CO2 Adsorbents for the Enhancement of Amine Efficiency. J Environ Chem Eng 9:106709. https://doi.org/10.1016/j.jece.2021.106709
36. Raganati F, Alfe M, Gargiulo V, et al (2018) Isotherms and thermodynamics of CO2 adsorption on a novel carbon-magnetite composite sorbent. Chem Eng Res Des 134:540–552. https://doi.org/10.1016/j.cherd.2018.04.037
37. Rahafza N, Manap A, Shamsudin R, et al (2018) Adsorption isotherm and kinetic study of gas-solid system of formaldehyde on oil palm mesocarp bio-char : Pyrolysis effect. J Environ Chem Eng 6:970–983. https://doi.org/10.1016/j.jece.2017.12.067
38. Rani S, Prusty BK, Pal SK (2018) Adsorption kinetics and diffusion modeling of CH4 and CO2 in Indian shales. Fuel 216:61–70. https://doi.org/10.1016/j.fuel.2017.11.124
39. Rojek T, Gubler L, Nasef MM, et al (2017) Polyvinylamine containing adsorbent by radiation induced grafting of N-vinylformamide onto UHMWPE films and hydrolysis for CO 2 capture. Ind Eng Chem Res 56:5925–5934
40. Schell J, Casas N, Pini R, Mazzotti M (2012) Pure and binary adsorption of CO 2, H 2, and N 2 on activated carbon. Adsorption 18:49–65. https://doi.org/10.1007/s10450-011-9382-y
41. Sharif J, Mohamad SF, Fatimah Othman NA, et al (2013) Graft copolymerization of glycidyl methacrylate onto delignified kenaf fibers through pre-irradiation technique. Radiat Phys Chem 91:125–131. https://doi.org/10.1016/j.radphyschem.2013.05.035
42. Shi L, Yuan H, Wu F, et al (2021) Robust “dry amine” solid CO2 sorbent synthesized by a facile, cost-effective and environmental friendly pathway. Chem Eng J 404:126447. https://doi.org/10.1016/j.cej.2020.126447

43. Shoushtari AM, Abdouss M, Rahmani S, et al (2012) Nano-Structral Surface Modified Polypropylene Nonwoven as Anion Absorbent by Amination of Plasma Activated Acrylic Acid Grafted Fiber. 11th World Filtr Congr 1–10
44. Tran HN, You SJ, Chao HP (2016) Thermodynamic parameters of cadmium adsorption onto orange peel calculated from various methods: A comparison study. J Environ Chem Eng 4:2671–2682. https://doi.org/10.1016/j.jece.2016.05.009
45. Ullah R, Atilhan M, Aparicio S, et al (2015) Insights of CO2adsorption performance of amine impregnated mesoporous silica (SBA-15) at wide range pressure and temperature conditions. Int J Greenh Gas Control 43:22–32. https://doi.org/10.1016/j.ijggc.2015.09.013
46. Vosoughi M, Maghsoudi H, Gharedaghi S (2021) Ion-exchanged ETS-10 adsorbents for CO2/CH4 separation: IAST assisted comparison of performance with other zeolites. J Nat Gas Sci Eng 88:103862. https://doi.org/10.1016/j.jngse.2021.103862
47. Wang P, Sun Q, Zhang Y, Cao J (2019) Synthesis of zeolite 4A from kaolin and its adsorption equilibrium of carbon dioxide. Materials (Basel) 12:1–12. https://doi.org/10.3390/ma12091536
48. Xu C, Yu G, Yuan J, et al (2020) Microporous organic polymers as CO2 adsorbents: advances and challenges. Mater Today Adv 6:. https://doi.org/10.1016/j.mtadv.2019.100052
49. Xu T, Wu Q, Chen S, Deng M (2015) Preparation of polypropylene based hyperbranched absorbent fibers and the study of their adsorption of CO2. RSC Adv 5:32902–32908. https://doi.org/10.1039/C5RA02182K
50. Yano K, Setoyama N, Fukumori K (2020) Investigation of Non-Thermodynamical CO₂ Adsorption Behavior for Amine-Modified Nanoporous Silica. Adv Mater Phys Chem 10:53–62. https://doi.org/10.4236/ampc.2020.103005
51. Zhao P, Yin Y, Xu X, et al (2022) Facile fabrication of mesoporosity silica as support for solid amine CO2 adsorbents with enhanced adsorption capacity and kinetics. Energy 253:124162. https://doi.org/10.1016/j.energy.2022.124162
52. Zhao P, Zhang G, Sun Y, Xu Y (2017) CO2Adsorption Behavior and Kinetics on Amine-Functionalized Composites Silica with Trimodal Nanoporous Structure. Energy and Fuels 31:12508–12520. https://doi.org/10.1021/acs.energyfuels.7b02292
53. Zhao P, Zhang G, Yan H, Zhao Y (2020) The latest development on amine functionalized solid adsorbents for post-combustion CO2 capture: Analysis review. Chinese J Chem Eng. https://doi.org/10.1016/j.cjche.2020.11.028
54. Zohdi S, Anbia M, Salehi S (2019) Improved CO2 adsorption capacity and CO2/CH4 and CO2/N2 selectivity in novel hollow silica particles by modification with multi-walled carbon nanotubes containing amine groups. Polyhedron 166:175–185. https://doi.org/10.1016/j.poly.2019.04.001
55. Zubair NA, Nasef MM, Mohamad NA, et al (2020) Kinetic studies of radiation induced grafting of N-vinylformamide onto polyethylene/polypropylene fibrous sheets and testing its hydrolysed copolymer for CO2 adsorption. Radiat Phys Chem 171:. https://doi.org/10.1016/j.radphyschem.2020.108727

Figures

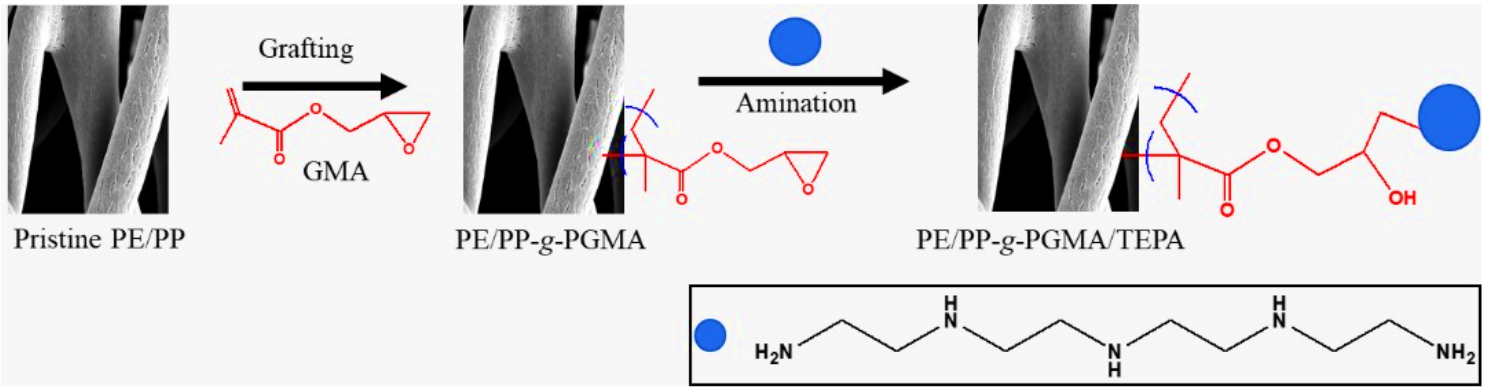

Figure 1

Schematic representation for preparation of fibrous adsorbent (PE/PP-g-PGMA/TEPA) by RIGC of GMA on PE/PP sheet and subsequent immobilization of TEPA.

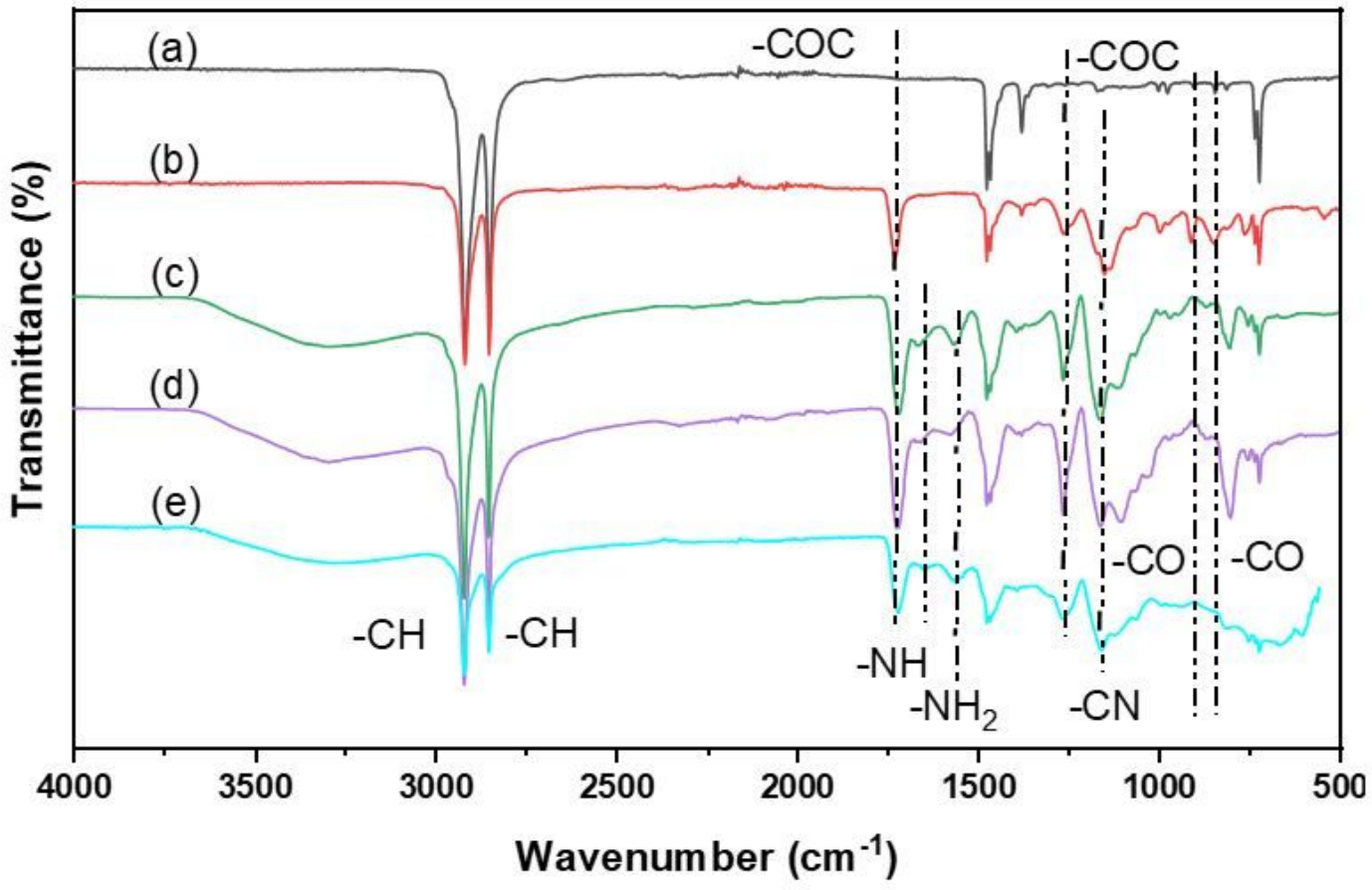

Figure 2

FTIR spectra of: a) pristine PE/PP, b) PE/PP-*g*-PGMA, c) PE/PP-*g*-PGMA/EDA, d) PE/PP-*g*-PGMA/DETA, and e) PE/PP-*g*-PGMA/TEPA fibrous sheets.

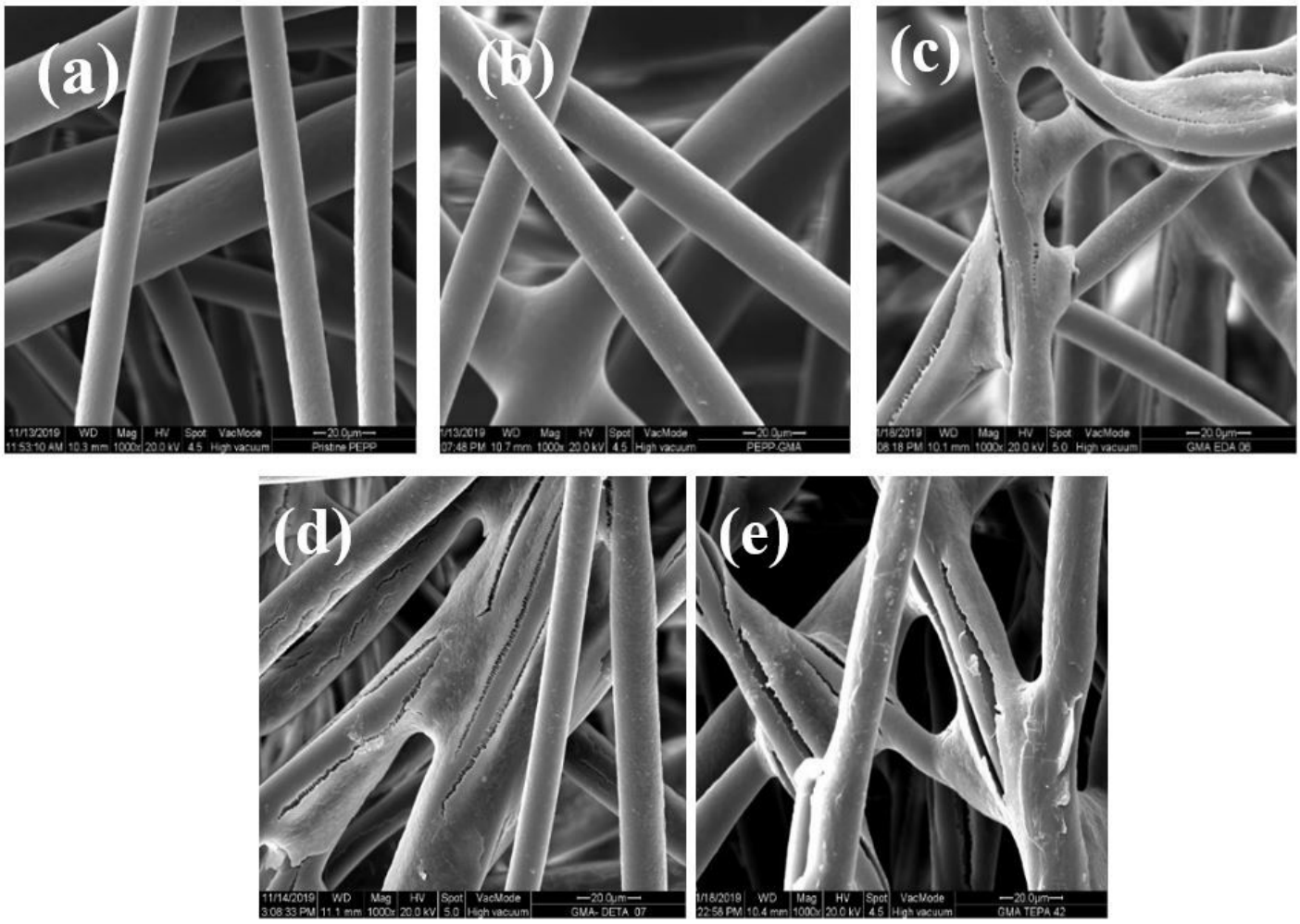

Figure 3

SEM images of: a) pristine PE/PP, b) PE/PP-*g*-PGMA, c) PE/PP-*g*-PGMA/EDA, d) PE/PP-*g*-PGMA/DETA, and e) PE/PP-*g*-PGMA/TEPA fibrous sheets.

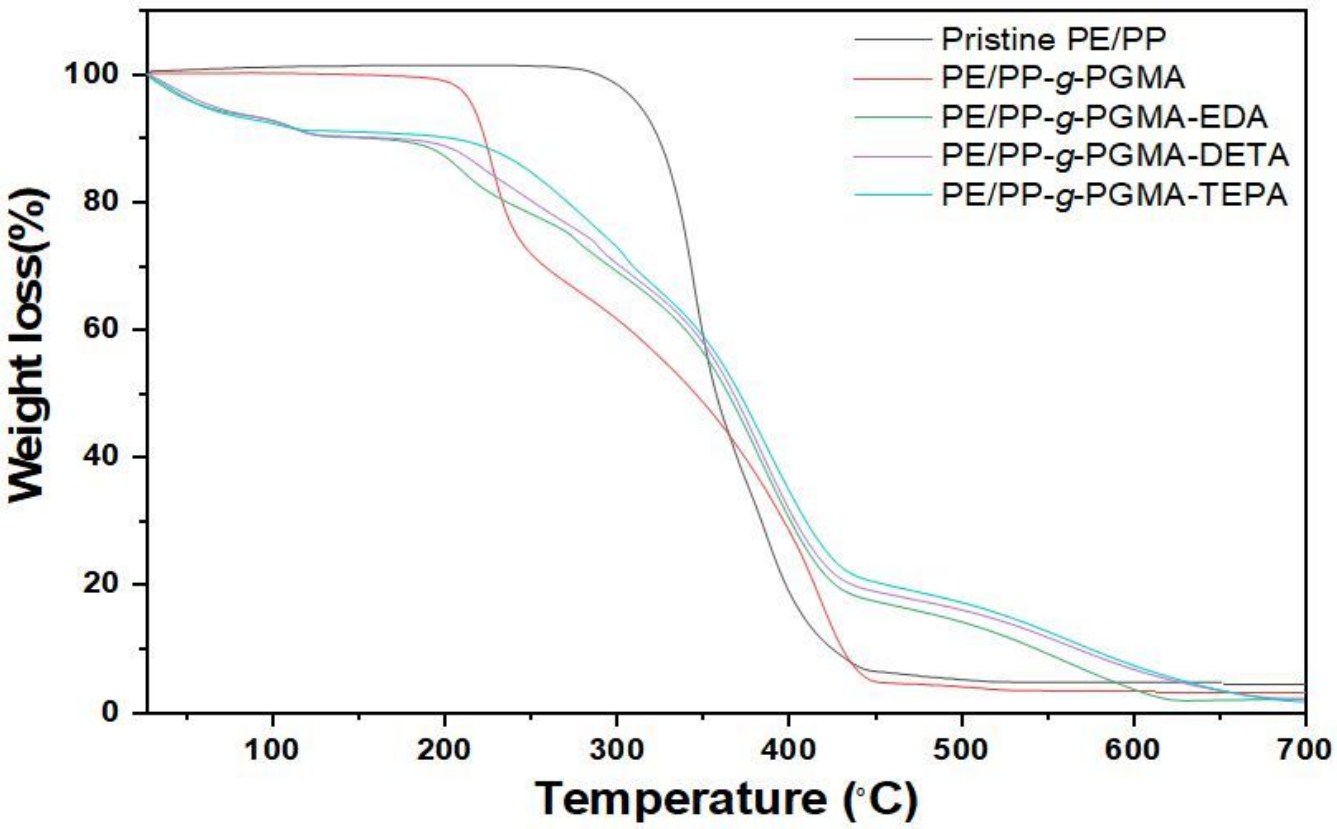

Figure 4

TGA thermograms of pristine PE/PP (black), PE/PP-*g*-PGMA (red), PE/PP-*g*-PGMA/EDA (green), PE/PP-*g*-PGMA/DETA (purple), and PE/PP-*g*-PGMA/TEPA (blue) fibrous sheets.

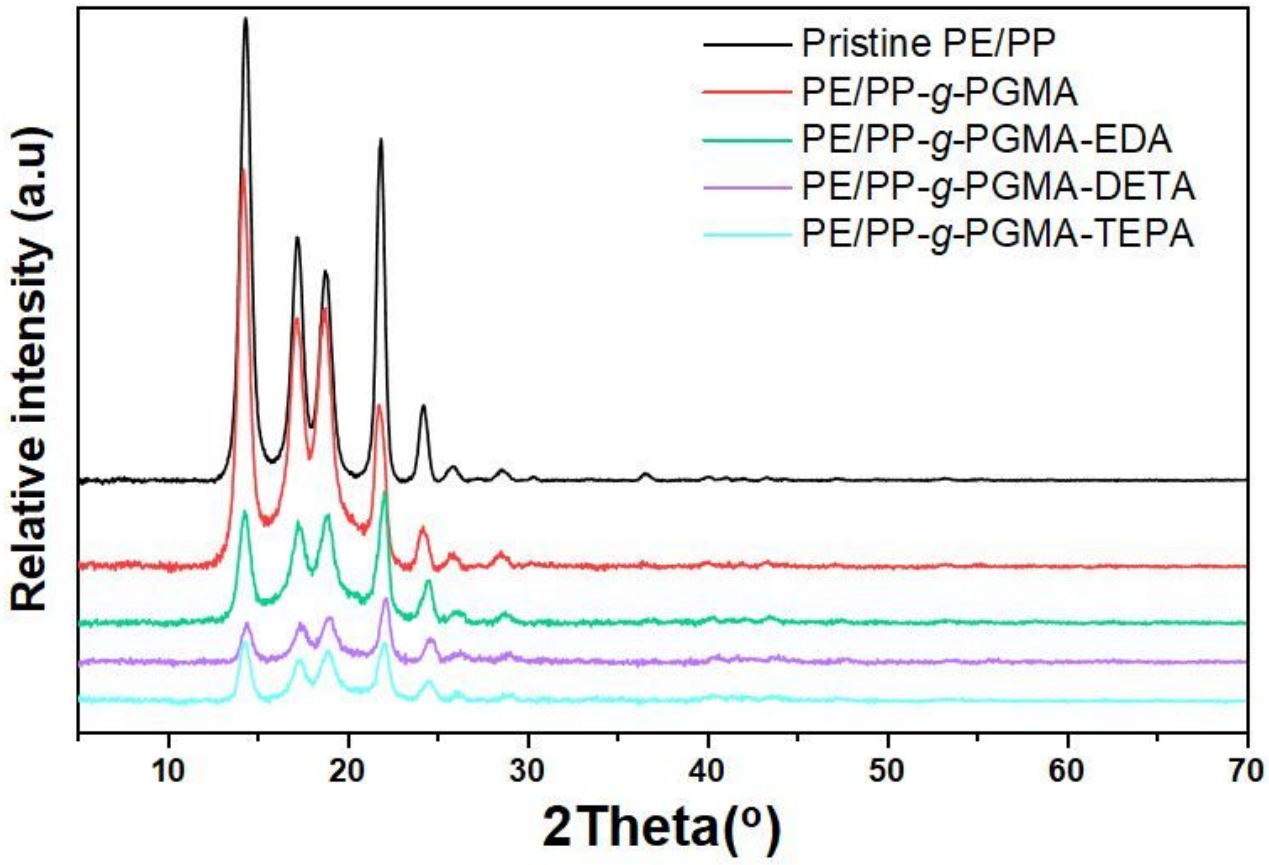

Figure 5

XRD diffractograms of pristine PE/PP (black), PE/PP-*g*-PGMA (red), PE/PP-*g*-PGMA/EDA (green), PE/PP-*g*-PGMA/DETA (purple), and PE/PP-*g*-PGMA/TEPA (blue) fibrous sheets.

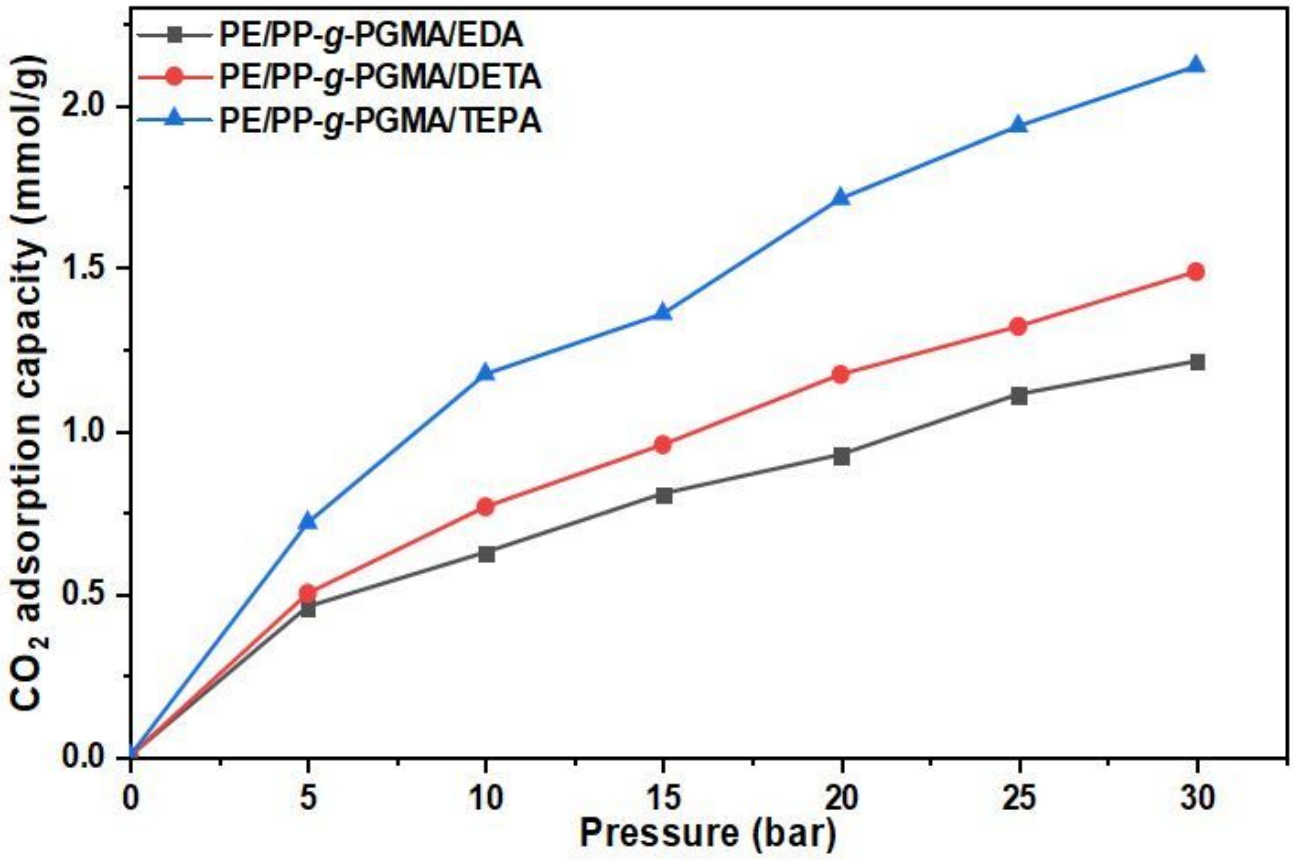

Figure 6

Variation of CO_2 adsorption capacity with pressure on adsorbents containing different amine types (EDA, DETA, and TEPA).

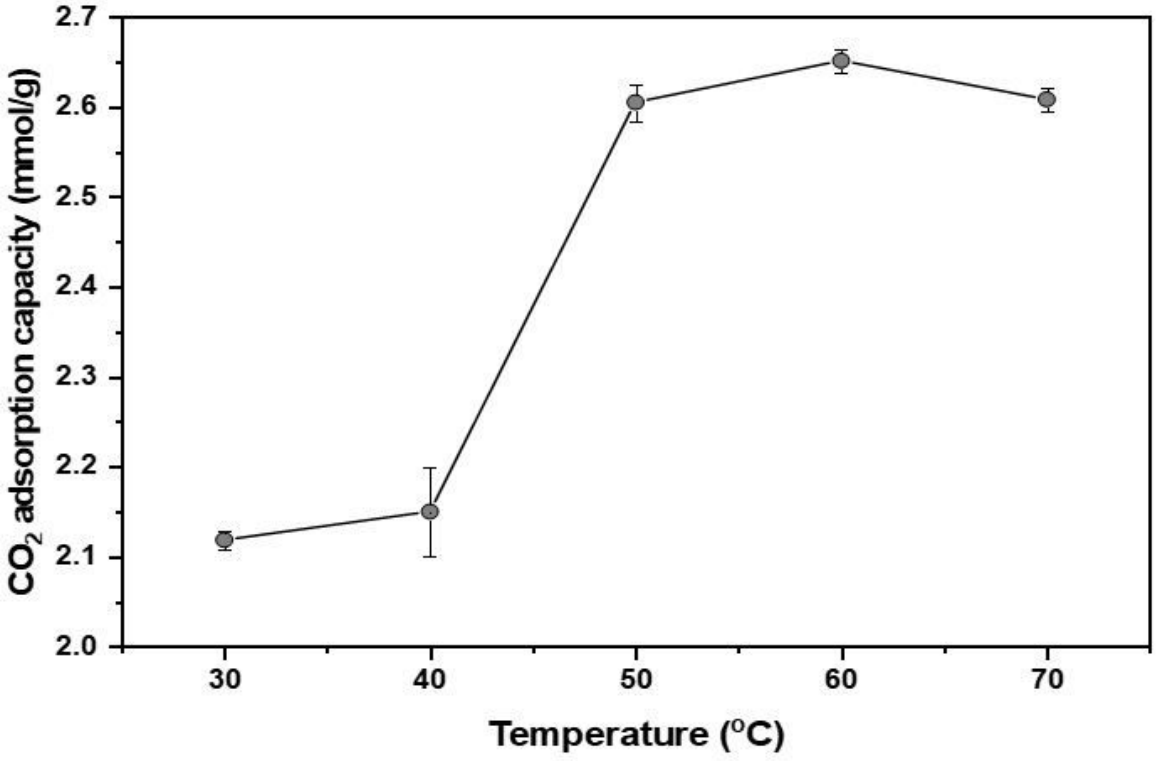

Figure 7

Variation of adsorption capacity of pure CO_2 on PE/PP-*g*-PGMA/TEPA with temperature at 30 bar.

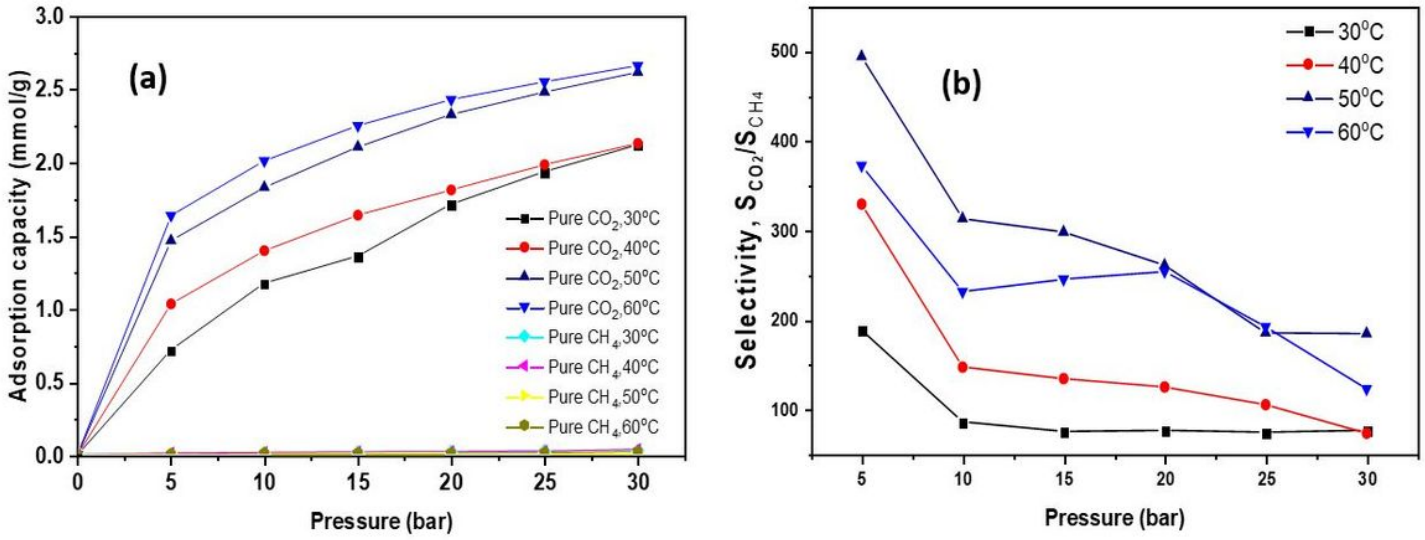

Figure 8

Effect of pressure on: a) adsorption capacity of pure CO_2 and CH_4 gases and b) selectivity of CO_2 over CH_4 at different temperatures.

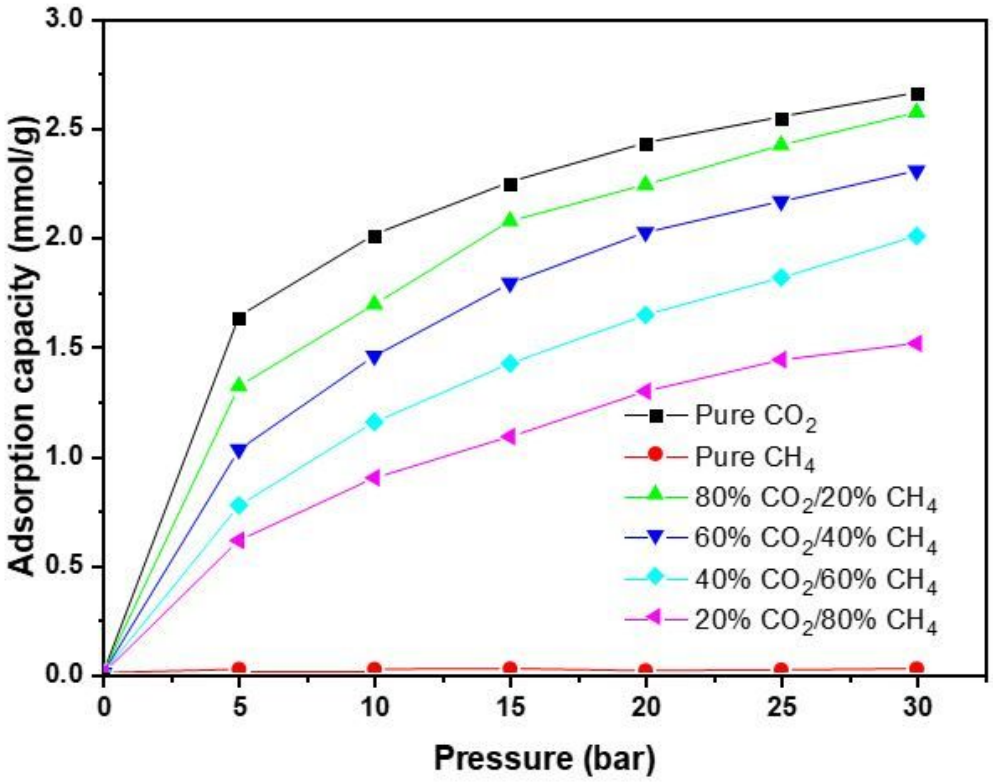

Figure 9

Variation of CO_2 adsorption capacity with pressure for at different CO_2/CH_4 gas compositions on PE/PP-*g*-PGMA/TEPA adsorbent.

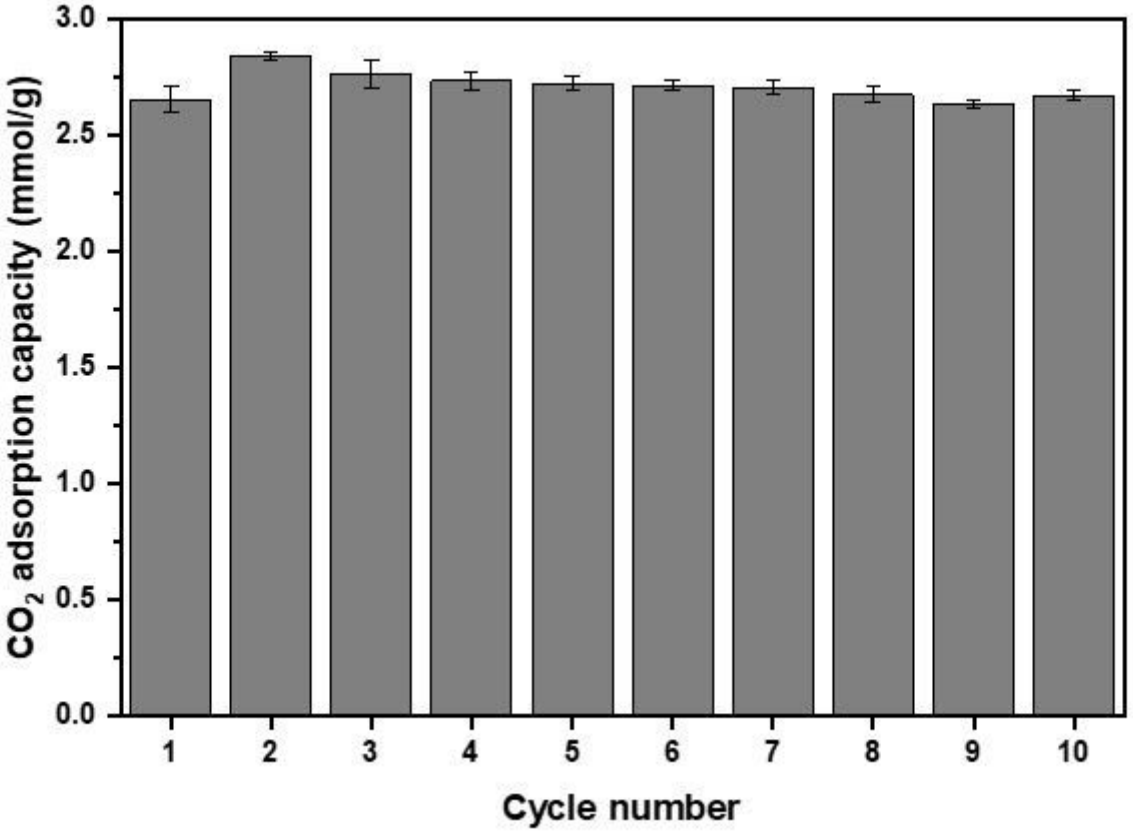

Figure 10

The effect of number of adsorption/desorption cycles on the adsorption capacity of pure CO_2 on PE/PP-g-PGMA/TEPA adsorbent.

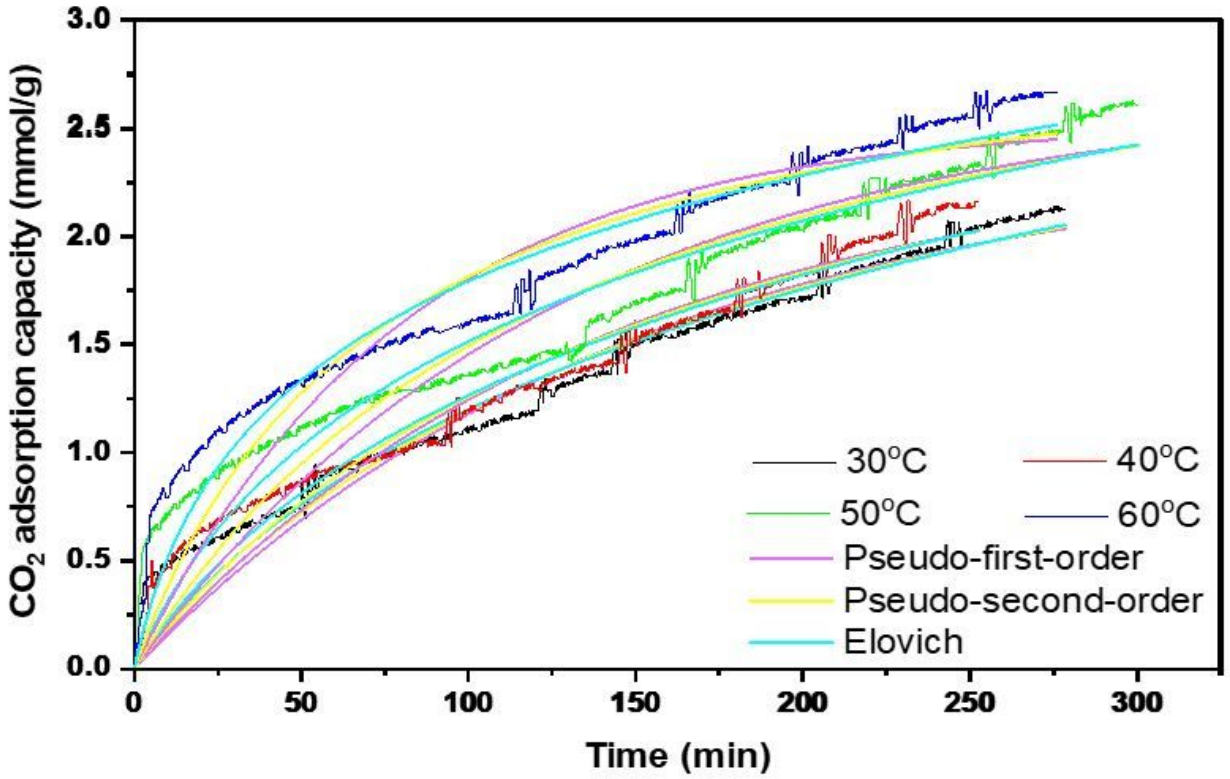

Figure 11

Fitting of CO_2 adsorption experimental data to three different kinetic models at 30, 40, 50, and 60 °C.

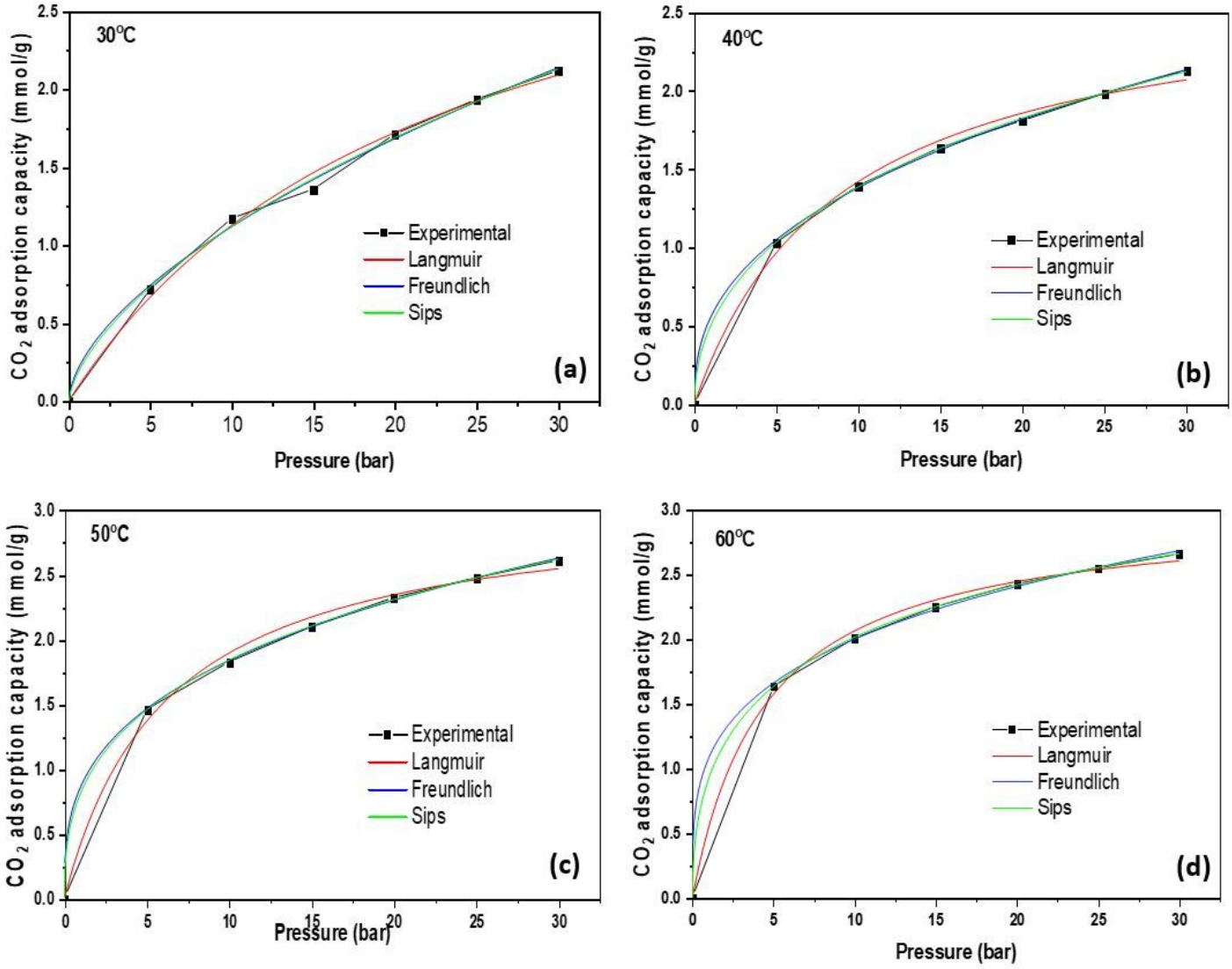

Figure 12

Adsorption isotherms and fitting curve for the two and three parameters isotherm model at different temperatures for PE/PP-*g*-PGMA/TEPA.

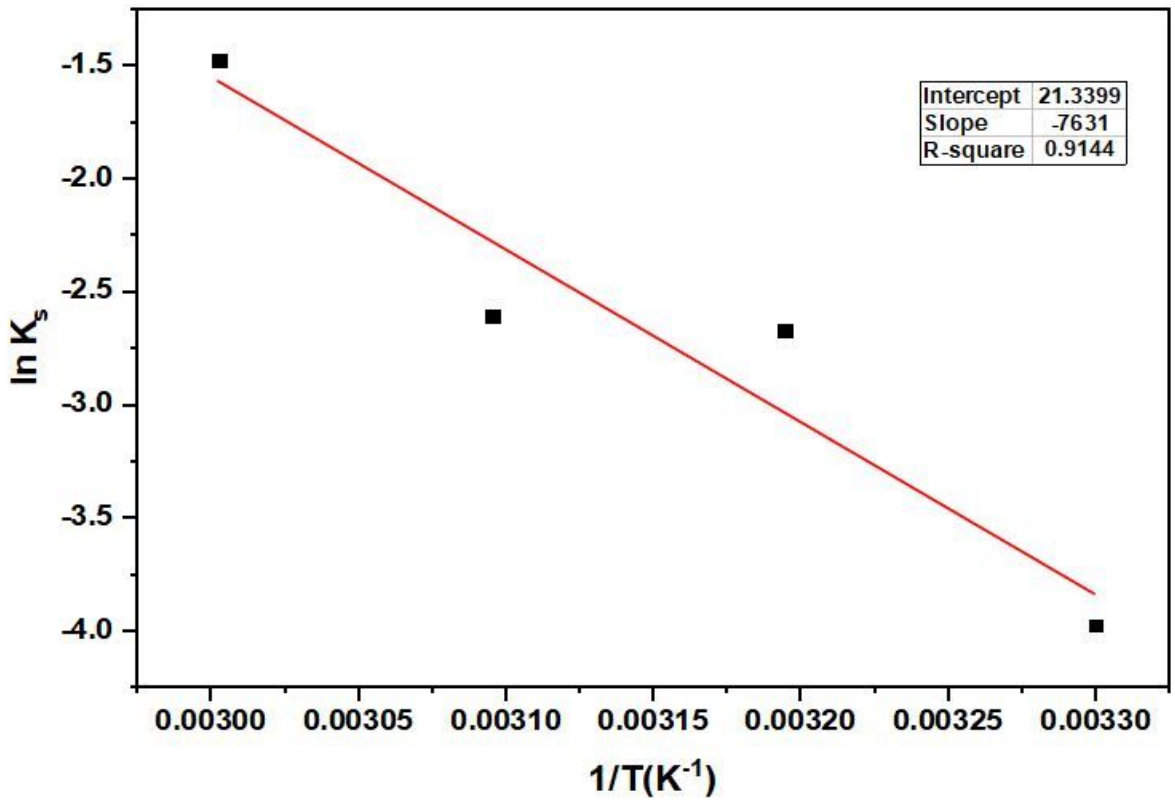

Figure 13

Van't Hoff plot for adsorption CO_2 on PE/PP-*g*-PGMA/TEPA adsorbent